Available online at www.sciencedirect.com
ScienceDirect
International Journal of Heat and Mass Transfer 51 (2008) 586–596
International Journal of HEAT and MASS TRANSFER
www.elsevier.com/locate/ijhmt

Simplified model and lattice Boltzmann algorithm for microscale electro-osmotic flows and heat transfer

Yong Shi, T.S. Zhao *, Zhaoli Guo

Department of Mechanical Engineering, The Hong Kong University of Science and Technology, Clear Water Bay, Kowloon, Hong Kong, China

Available online 27 June 2007

Abstract

The extremely small length scale of the electric double layer (EDL) of electro-osmotic flows (EOF) in a microchannel makes it difficult to simulate such flows and associated thermal behaviors. A feasible solution to this problem is to neglect the details in the thin EDL and replace its effects on the bulk flow and heat transfer with effective velocity-slip and temperature-jump boundary conditions outside the EDL. In this paper, by carrying out a scale analysis on the fluid flow and heat transfer in the thin EDL, we analytically obtain the velocity and the temperature at the interface between the EDL and the bulk flow region. The Navier–Stokes equations and the conservation equation of energy, along with the interfacial velocity and temperature as the velocity-slip and temperature-jump boundary conditions, form a simple model for the electro-osmotic flows with thermal effects in a microchannel with a thin EDL. We use the double distribution function lattice Boltzmann algorithm to solve this model and found that numerical results are in good agreement with those by the conventional complete model with inclusion of the EDL, particularly for the cases when channel size is about 400 times larger than the Debye length. Moreover, we found that the present model can substantially reduce the computational time by four to five times of that using the conventional complete model. Therefore, the simplified model proposed in this work is an efficient tool for simulating electro-osmosis-based microfluidic systems.

Keywords: Electro-osmotic flows; Heat transfer; Lattice Boltzmann method; Microscale

1. Introduction

The electro-osmotic flow (EOF) has received considerable attention with the rapid development in microfabrication technologies over the last decade. In many scientific and engineering applications, various innovative microfluidic systems use the electro-osmosis to pump liquids [1–15] or control flows [16,17,24]. In comparison with other mechanical microfluidic systems, the most important advantage of the electro-osmosis-based microfluidic systems is that they do not require any moving components. This greatly simplifies the design and fabrication of microfluidic systems and improves the reliability of their operation. In various electro-osmosis-based microfluidic systems, a microchannel is the simplest and primarily-used component. Therefore, the understanding of the electro-osmotic flow and associated thermal behavior in microchannels is not only fundamentally important, but also essential for the design of microfluidic systems.

A number of papers have reported on the study of the EOFs in microchannels over recent years. Generally, the models reported in the previous works fall into two categories: the complete model [18–23] and the model with exclusion of the electric double layer (EDL) [24–33]. The complete model, constructed based on the EDL theory developed by Gouy [34], consists of three coupling differential equations: the Poisson–Boltzmann equation, the Navier–Stokes equation and the conservation equation of energy, which describe the change of the electric potential, the motion of the fluid and the distribution of the temperature, respectively [19–23]. Moreover, in the complete model, the conventional non-slip boundary condition for fluid flow and the Dirichlet boundary conditions with a given wall

* Corresponding author. Tel.: +852 2358 8647; fax: +852 2358 1543.
E-mail address: metzhao@ust.hk (T.S. Zhao).

0017-9310/$ - see front matter © 2007 Elsevier Ltd. All rights reserved.
doi:10.1016/j.ijheatmasstransfer.2007.05.003

temperature T_0 and a zeta potential ζ for temperature and electric potential distribution are usually specified, respectively. Therefore, the complete model essentially covers the entire channel including both the EDL and the bulk flow region. However, the EDL thickness, represented by the Debye length, λ, is extremely small. For example, for a symmetric univalent electrolyte at 25 °C, its Debye length is only about 1.0 nm for the concentration of 10^2 mol/m^3 and 10.0 nm for 1 mol/m^3 [35]. This means that for a microchannel with its width, h, in the range of several to several hundreds of micrometers, the length ratio $\gamma = h/\lambda$, is up to 10^2–10^5. For this reason, when the complete model is used, an extremely fine grid is needed to simulate the EDL, making the total number of grids in the entire channel extremely large. For instance, in an EOF system with $\gamma = 500$ as shown in Fig. 1, five grid nodes distributing across the EDL region will lead to a total of about 2500 grid nodes in y direction of the entire channel. Thus, the numerical simulation of the EOFs in microchannels based on the complete model requires a prohibitive amount of memory and consumes an extremely long computational time.

To overcome the above-mentioned problem, efforts have been made to simplify the mathematical description for isothermal EOF systems with a large γ [24–33]. Generally, an EOF can be divided into two flow regions: the EDL and the bulk flow region. When channel width is much larger than the Debye length, it is found the electro-kinetic effect is confined in the EDL and the bulk EOF behaves like the flow of an electro-neutrality fluid [24–31]. This indicates that in the bulk flow region, the Poisson–Boltzmann equation can be eliminated and the complex electro-osmotic body force term in the Navier–Stokes equations can also be removed. Moreover, the EDL in such a case is rather thin and the bulk flow is dominant in the entire channel. As a result, it can be well justified to neglect the transport details in the EDL and replace its electro-kinetic effect on the bulk flow by effective slip boundary conditions. In line of this idea, the model with exclusion of the EDL for EOFs with a large γ has been developed in the literature [24–33]. Clearly, such a model is much simpler than the complete model, and thereby the corresponding computer memory and the computational time being substantially reduced.

For isothermal EOF systems, the model with exclusion of the EDL usually uses the Helmholtz–Smoluchowski (HS) velocity, $u_s = -\varepsilon\zeta E/\mu$, as a velocity-slip boundary condition at the solid wall, where ε, E and μ represent the dielectric constant, the applied electric field strength and the viscosity, respectively [24–30]. This HS velocity is actually the velocity at the interface between the EDL and the bulk flow region derived under the assumption that both the velocity and electric potential gradients in the bulk flow region are zero [26]. It is treated as a velocity-slip boundary condition only when channel width is much larger than the Debye length. Recently, Dutta and Beskok [32,33] have found that the HS velocity as a boundary condition can be extended to the isothermal mixed electro-osmotic/pressure driven flows with a finite EDL. In this case, it can be obtained by extrapolating the bulk flow velocity onto the solid wall.

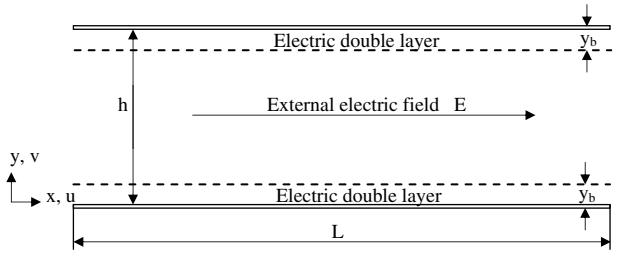

Fig. 1. The geometric configuration of the microchannel.

Most previous investigations have been confined to the isothermal EOFs in microchannels. Relatively, few efforts have been made to model the EOF with thermal effects and examine the HS velocity as a slip boundary condition under thermal conditions. In fact, a non-uniform temperature distribution occurs in many practical electro-osmosis-based microfluidic systems [36–38], and such a temperature distribution exerts a significant impact on the performance of the systems. For example, Zhao and Liao [23] have investigated the thermal effects on electro-osmotic pumping of liquids in microchannels. They found that the performance of EOF pumps under thermal conditions is substantially different from that under isothermal conditions. Moreover, other works reported that the temperature gradient in microchannels also crucially influences the analyte dispersion in electro-kinetic separation [39,40] and the temperature sensitive chemical process, such as the DNA amplification in the micropolymerase chain reaction (PCR) [41,42]. Therefore, to accurately describe these electro-kinetic phenomena, it is needed to develop a simplified model with exclusion of the EDL for the EOFs with thermal effects. Generally, a temperature gradient within microchannels might arise from two circumstances. First, Joule heating associated with an applied electric voltage to the fluid may be significant when the applied voltage and the specific electric conductivity are sufficiently high [37,38]. Secondly, the fluid flow in channels is not in a thermal equilibrium with the ambient condition when it is cooled or heated by the surroundings. Under these circumstances, the temperature gradient results in variable fluid properties [43] and affects the charge distribution in the channel. This causes the fluid velocity in thermal EOFs to differ from that under isothermal conditions. Therefore, it can be expected that the conventional HS velocity obtained under the isothermal conditions may no longer be sufficiently accurate for the EOFs with thermal effects.

The objective of this work is to obtain a simplified model with exclusion of the EDL for simulating the EOFs with thermal effects in microchannels. To this end, we perform a scale analysis to the complete model consisting of the Poisson–Boltzmann equation, the Navier–Stokes equations and the conservation equation of energy in the EDL and come up with the simplified equations. By integrating these simplified equations over the EDL, we obtain the velocity and temperature at the interface between the

EDL and the bulk flow region. Unlike previous studies, we do not extrapolate these interfacial conditions onto the wall to obtain those fictitious slip boundary conditions. Instead, considering the fact the EDL is rather small and the bulk flow is dominant in the entire channel, we directly approximate the thermal EOFs by the bulk flow with these interfacial conditions in this work. More specifically, we use the Navier–Stokes equations and the conservation equation of energy, with the interfacial velocity and temperature as the velocity-slip and temperature-jump boundary conditions, to form a simple model for the EOFs with thermal effects in microchannels. We apply the double distribution function lattice Boltzmann algorithm [44] to numerically solve this model and compare the numerical results with those obtained by the complete model with inclusion of the EDL [45]. The rest of the article is organized as follows: we first present the conventional complete model with inclusion of the EDL for thermal EOFs (Section 2). We then simplify the complete model and obtain a simple model with the velocity-slip and temperature-jump boundary conditions for thermal EOFs in microchannels (Section 3). Next, we introduce the double distribution thermal lattice Boltzmann algorithm for solving the proposed model (Section 4). In Section 5, the numerical results are compared with those obtained by the complete model under isothermal/thermal conditions. Finally, the conclusions drawn from this work are presented in Section 6.

2. The complete model with inclusion of the EDL

In this section, we outline the complete model with inclusion of the EDL. Without losing generality, we consider the electro-osmotic flow in a two-dimensional microchannel shown in Fig. 1, which is driven by an external electric field applied at the both ends. When the dielectric solid surface of the channel is in contact with an electrolytic solution, the so-called electric double layer forms due to the interaction of the ionized solution with the static charges on the dielectric surfaces. The corresponding electric potential of ions, φ, is related to the net electric charge density in the solution, ρ_e, via the Poisson equation:

$$\frac{\partial}{\partial x}\left(\varepsilon\frac{\partial\varphi}{\partial x}\right)+\frac{\partial}{\partial y}\left(\varepsilon\frac{\partial\varphi}{\partial y}\right)=-\rho_e, \tag{1}$$

where ε is the permittivity of the electrolytic solution and depends on temperature. The net electric charge density, ρ_e, is usually assumed to be distributed in the channel subject to the Boltzmann distribution. For a symmetric electrolyte, ρ_e is given by [26]

$$\rho_e=-2n_\infty ze\sinh\left(\frac{ze\varphi}{k_BT}\right), \tag{2}$$

where n_∞ is the ion density in the bulk flow. The thickness of the EDL is characterized by the Debye length [46]:

$$\lambda=\sqrt{\frac{\varepsilon(T_0)k_BT_0}{2n_\infty e^2z^2}}, \tag{3}$$

where e is the elementary charge, z is the valence of ions, and T_0 is the reference temperature, defined to be the wall temperature in this work. Under the effect of the applied electric field (x direction in Fig. 1), the ionized incompressible flow with the electro-osmotic body force is governed by the Navier–Stokes equations:

$$\rho\left(\frac{\partial u}{\partial t}+u\frac{\partial u}{\partial x}+v\frac{\partial u}{\partial y}\right)=-\frac{\partial p}{\partial x}+\frac{\partial}{\partial x}\left(\mu\frac{\partial u}{\partial x}\right)+\frac{\partial}{\partial y}\left(\mu\frac{\partial u}{\partial y}\right)+\rho_eE, \tag{4}$$

$$\rho\left(\frac{\partial v}{\partial t}+u\frac{\partial v}{\partial x}+v\frac{\partial v}{\partial y}\right)=-\frac{\partial p}{\partial y}+\frac{\partial}{\partial x}\left(\mu\frac{\partial v}{\partial x}\right)+\frac{\partial}{\partial y}\left(\mu\frac{\partial v}{\partial y}\right), \tag{5}$$

where u, v are the component of the fluid velocity in x direction and y direction, E is the component of the electric field strength $\boldsymbol{E}$ in x direction, and p is the pressure. In Eqs. (4) and (5), the fluid density, ρ, is assumed to be constant, whereas the viscosity, μ, is a temperature-dependent variable. Moreover, the conservation of mass requires that

$$\frac{\partial u}{\partial x}+\frac{\partial v}{\partial y}=0. \tag{6}$$

In addition, due to Joule heating and heat transfer from/to the surroundings, there exist temperature gradients in the electro-osmotic flow. Assuming that the viscous dissipation and the compressible work are negligibly small, the temperature distribution is governed by the conservation equation of energy:

$$\frac{\partial T}{\partial t}+u\frac{\partial T}{\partial x}+v\frac{\partial T}{\partial y}=\frac{\partial}{\partial x}\left(\frac{k}{\rho c_p}\frac{\partial T}{\partial x}\right)+\frac{\partial}{\partial y}\left(\frac{k}{\rho c_p}\frac{\partial T}{\partial y}\right)+\frac{KE^2}{\rho c_p}, \tag{7}$$

where T is temperature, c_p is the specific heat, k and K are the thermal conductivity and the electric conductivity of the electrolytic solution, respectively. In this work, c_p is assumed to be constant, whereas k and K are temperature-dependent variables. Eqs. (1) and (4)–(7) describe the thermal incompressible EOF in microchannels. The corresponding dimensionless form of Eqs. (1) and (4)–(7) are given by

$$\frac{\partial}{\partial X}\cdot\left(\bar{\varepsilon}\frac{\partial\Phi}{\partial X}\right)+\frac{\partial}{\partial Y}\cdot\left(\bar{\varepsilon}\frac{\partial\Phi}{\partial Y}\right)=\beta\sinh\left(\frac{\alpha\Phi}{1+\theta}\right), \tag{8}$$

$$\frac{\partial U}{\partial X}+\frac{\partial V}{\partial Y}=0, \tag{9}$$

$$\frac{\partial U}{\partial\tau}+U\frac{\partial U}{\partial X}+V\frac{\partial U}{\partial Y}=-\frac{1}{Re}\frac{\partial P}{\partial X}+\frac{1}{Re}\left[\frac{\partial}{\partial X}\left(\bar{\mu}\frac{\partial U}{\partial X}\right)+\frac{\partial}{\partial Y}\left(\bar{\mu}\frac{\partial U}{\partial Y}\right)\right]+\frac{\beta}{Re}\sinh\left(\frac{\alpha\Phi}{1+\theta}\right), \tag{10}$$

$$\frac{\partial V}{\partial\tau}+U\frac{\partial V}{\partial X}+V\frac{\partial V}{\partial Y}=-\frac{1}{Re}\frac{\partial P}{\partial Y}+\frac{1}{Re}\left[\frac{\partial}{\partial X}\left(\bar{\mu}\frac{\partial V}{\partial X}\right)+\frac{\partial}{\partial Y}\left(\bar{\mu}\frac{\partial V}{\partial Y}\right)\right], \tag{11}$$

and

$$\frac{\partial\theta}{\partial\tau}+U\frac{\partial\theta}{\partial X}+V\frac{\partial\theta}{\partial Y}=\frac{1}{RePr}\left[\frac{\partial}{\partial X}\left(\bar{k}\frac{\partial\theta}{\partial X}\right)+\frac{\partial}{\partial Y}\left(\bar{k}\frac{\partial\theta}{\partial Y}\right)\right]+\frac{J}{RePr}\overline{K}, \tag{12}$$

where the dimensionless quantities are defined as follows: $\Phi=\varphi/\zeta$, with ζ representing the zeta potential; $X=x/h$ and $Y=y/h$ with h representing the channel width; $(U,V)=(u,v)/u_s$, with $u_s=-\varepsilon(T_0)\zeta E/\mu$ being the HS velocity; $\tau=tu_s/h$; $\theta=(T-T_0)/T_0$; and $P=ph/(\mu u_s)$. In addition, $Re=\rho u_s h/\mu(T_0)$ is the Reynolds number, $Pr=\mu(T_0)c_p/k(T_0)$ is the Prandtl number, $J=K(T_0)h^2E^2/[k(T_0)T_0]$ is the Joule number, $\alpha=ez\zeta/(k_BT_0)$ is the ionic energy parameter, and $\beta=h^2/(\alpha\lambda^2)$ relates the thickness of the EDL to the channel width. All the dimensionless forms of the temperature-dependent fluid properties in the above equations are defined as $\bar{\varepsilon}(T)=\varepsilon(T)/\varepsilon(T_0)$, $\bar{\mu}(T)=\mu(T)/\mu(T_0)$, $\bar{k}(T)=k(T)/k(T_0)$ and $\overline{K}(T)=K(T)/K(T_0)$.

3. The simplified model with exclusion of the EDL

Eqs. (8)–(12) give a full description of the flow and heat transfer behavior of the electrolytic solution in the entire channel domain, including both the bulk flow region and the EDL. Typically, however, the EDL thickness (on the nanometer) is much thinner than channel width (on the micrometer), i.e., $\lambda\ll h$. A numerical solution to Eqs. (8)–(12) in the entire channel domain consisting of these different length scales would require a prohibitive amount of memory and computational time. Hence, it is essential to simplify the complete model presented in the preceding section. It should be recognized that when channel width is much larger than the Debye length, the electro-kinetic effect on the fluid flow and heat transfer behavior is confined within a rather narrow region near channel walls, meaning that in the bulk flow region, the electric potential of ion, φ, and the corresponding net charge density, ρ_e, are negligibly small. For this reason, the Poisson–Boltzmann equation (8) for the electric potential is no longer required and the electro-osmotic body force in the Navier–Stokes equations also vanishes. Hence, based on Eqs. (8)–(12), the governing equations for thermal electro-osmotic flows in the bulk flow region can be written as

$$\frac{\partial U}{\partial X}+\frac{\partial V}{\partial Y}=0, \tag{13}$$

$$\frac{\partial U}{\partial\tau}+U\frac{\partial U}{\partial X}+V\frac{\partial U}{\partial Y}=-\frac{1}{Re}\frac{\partial P}{\partial X}+\frac{1}{Re}\left[\frac{\partial}{\partial X}\left(\bar{\mu}\frac{\partial U}{\partial X}\right)+\frac{\partial}{\partial Y}\left(\bar{\mu}\frac{\partial U}{\partial Y}\right)\right], \tag{14}$$

$$\frac{\partial V}{\partial\tau}+U\frac{\partial V}{\partial X}+V\frac{\partial V}{\partial Y}=-\frac{1}{Re}\frac{\partial P}{\partial Y}+\frac{1}{Re}\left[\frac{\partial}{\partial X}\left(\bar{\mu}\frac{\partial V}{\partial X}\right)+\frac{\partial}{\partial Y}\left(\bar{\mu}\frac{\partial V}{\partial Y}\right)\right], \tag{15}$$

and

$$\frac{\partial\theta}{\partial\tau}+U\frac{\partial\theta}{\partial X}+V\frac{\partial\theta}{\partial Y}=\frac{1}{RePr}\left[\frac{\partial}{\partial X}\left(\bar{k}\frac{\partial\theta}{\partial X}\right)+\frac{\partial}{\partial Y}\left(\bar{k}\frac{\partial\theta}{\partial Y}\right)\right]+\frac{J}{RePr}\overline{K}. \tag{16}$$

The electro-kinetic effect in the EDL on the bulk flow and heat transfer behavior can be taken into account by the velocity and the temperature at the interface between the EDL and the bulk flow region, which can be obtained as follows.

Based on Eqs. (8)–(12), the governing equations for the EOF within the EDL can be written as

$$\bar{\varepsilon}_s\left(\frac{\partial^2\Phi}{\partial X^2}+\frac{h^2}{\lambda^2}\frac{\partial^2\Phi}{\partial\overline{Y}^2}\right)=\beta\sinh\left(\frac{\alpha\Phi}{1+\theta}\right), \tag{17}$$

$$\frac{\partial U}{\partial X}+\frac{\partial\overline{V}}{\partial\overline{Y}}=0, \tag{18}$$

$$\frac{\partial U}{\partial\tau}+U\frac{\partial U}{\partial X}+\overline{V}\frac{\partial U}{\partial\overline{Y}}=-\frac{1}{Re}\frac{\partial P}{\partial X}+\frac{\bar{\mu}_s}{Re}\left(\frac{\partial^2U}{\partial X^2}+\frac{h^2}{\lambda^2}\frac{\partial^2U}{\partial\overline{Y}^2}\right)+\frac{\beta}{Re}\sinh\left(\frac{\alpha\Phi}{1+\theta}\right), \tag{19}$$

$$\frac{\partial\overline{V}}{\partial\tau}+U\frac{\partial\overline{V}}{\partial X}+\overline{V}\frac{\partial\overline{V}}{\partial\overline{Y}}=-\frac{1}{Re}\frac{h^2}{\lambda^2}\frac{\partial P}{\partial\overline{Y}}+\frac{\bar{\mu}_s}{Re}\left(\frac{\partial^2\overline{V}}{\partial X^2}+\frac{h^2}{\lambda^2}\frac{\partial^2\overline{V}}{\partial\overline{Y}^2}\right), \tag{20}$$

and

$$\frac{\partial\theta}{\partial\tau}+U\frac{\partial\theta}{\partial X}+\overline{V}\frac{\partial\theta}{\partial\overline{Y}}=\frac{\bar{k}_s}{Re\,Pr}\left(\frac{\partial^2\theta}{\partial X^2}+\frac{h^2}{\lambda^2}\frac{\partial^2\theta}{\partial\overline{Y}^2}\right)+\frac{J\overline{K}_s}{Re\,Pr}, \tag{21}$$

where all the dimensionless variables are the same as those in Eqs. (8)–(12) except that the dimensionless length $\overline{Y}=y/\lambda$, and the dimensionless velocity component in y direction $\overline{V}=v/v_0$, with $v_0=u_s\lambda/h$ being determined by Eq. (18). Moreover, the temperature-dependent fluid properties in Eqs. (17)–(21) are evaluated at the temperature of the interface between the EDL and the bulk flow region, T_b, i.e., $\bar{\varepsilon}_b=\varepsilon(T_b)/\varepsilon(T_0)$, $\bar{\mu}_b=\mu(T_b)/\mu(T_0)$, $\bar{k}_b=k(T_b)/k(T_0)$ and $\overline{K}_b=K(T_b)/K(T_0)$, where the subscript 'b' denotes the interface between the EDL and the bulk flow region. Based on the facts that $h\gg\lambda$, $Re\ll1$, and the velocity only in x direction, Eqs. (17)–(21) can further be simplified as

$$\frac{\partial^2\Phi}{\partial\overline{Y}^2}=\frac{\lambda^2\beta\sinh[\alpha\Phi/(1+\theta)]}{h^2\bar{\varepsilon}_b}, \tag{22}$$

$$\bar{\mu}_b\frac{\partial^2U}{\partial\overline{Y}^2}+\frac{\lambda^2}{h^2}\beta\sinh\left(\frac{\alpha\Phi}{1+\theta}\right)=0, \tag{23}$$

$$\bar{k}_b\frac{\partial^2\theta}{\partial\overline{Y}^2}+\frac{\lambda^2}{h^2}J\overline{K}_b=0. \tag{24}$$

Eqs. (23) and (24) indicate that in the EDL, the external electric force is balanced by the viscous force in x direction while the internal Joule heating is transferred by the heat conduction in y direction. Substituting Eq. (22) into Eq. (23) and performing integration over the EDL, we obtain

$$U_b = \frac{\bar{\varepsilon}_b}{\bar{\mu}_b} - \frac{\bar{\varepsilon}_b \Phi_b}{\bar{\mu}_b} + \overline{Y}_b \frac{\lambda}{h} (\widetilde{\nabla} U \cdot \mathbf{n})_b + \frac{\bar{\varepsilon}_b \lambda}{\bar{\mu}_b h} \overline{Y}_b (\widetilde{\nabla} \Phi \cdot \mathbf{n})_b, \quad (25)$$

where U_b and Φ_b represent the dimensionless velocity and electric potential at the interface between the EDL and the bulk flow region, respectively; $\mathbf{n}$ represents the unity vector normal to the wall and pointing to the inside of the electrolytic solution; $\widetilde{\nabla} = \mathbf{i}\partial/\partial X + \mathbf{j}\partial/\partial Y$, with $\mathbf{i}$ and $\mathbf{j}$ representing the unity vector in x and y direction and $\overline{Y}_b$ is the thickness of the EDL scaled by λ. In Eq. (25), the first term on the right-hand side represents the dimensionless HS velocity evaluated at T_b and the last three terms correspond to the dimensionless electric potential, the dimensionless velocity gradient, and the dimensionless electric potential gradient at the interface between the EDL and the bulk flow region, respectively. Note that the dimensionless electric potential gradient, $(\widetilde{\nabla}\Phi \cdot \mathbf{n})$, can be expressed by the dimensionless velocity gradient of the pure EOF (i.e., $dP/dX = 0$) in microchannels, i.e.,

$$(\widetilde{\nabla}\Phi \cdot \mathbf{n}) = -\frac{\bar{\mu}_b}{\bar{\varepsilon}_b} (\widetilde{\nabla} U^e \cdot \mathbf{n}). \quad (26)$$

Therefore, with Eq. (26), Eq. (25) is reduced to

$$U_b = \frac{\bar{\varepsilon}_b}{\bar{\mu}_b} - \frac{\bar{\varepsilon}_b \Phi_b}{\bar{\mu}_b} + \overline{Y}_b \frac{\lambda}{h} \left(\widetilde{\nabla} U^p \cdot \mathbf{n} \right)_b, \quad (27)$$

where $U^p = U - U^e$, corresponding to the part of the bulk flow velocity driven by the pressure gradient. The magnitudes of the last two interfacial terms on the right-hand side of Eq. (27) depend upon the definition of the interface between the EDL and the bulk flow region. The electric potential can be obtained by solving Eq. (22). When the electrical energy is much smaller than the thermal energy of ion, viz. $|\alpha\Phi| \ll 1$, Eq. (22) can be simplified to

$$\frac{\partial^2 \Phi}{\partial \overline{Y}^2} = a^2 \Phi, \quad (28)$$

where $a = 1/\sqrt{\bar{\varepsilon}_b(1+\theta)}$. Eq. (28) represents the so-called Debye–Hückel approximation. For a univalent electrolytic solution at room temperature, the Debye–Hückel approximation holds when the magnitude of the zeta potential is less than 25 mV. It may be worth mentioning that the study of electro-osmotic flows without the Debye–Hückel approximation can be found elsewhere [47,48]. In addition to the Debye–Hückel approximation, since the thickness of the EDL is much smaller than channel width, we further assume $a = 1/\sqrt{\bar{\varepsilon}_b(1+\theta_b)}$, with θ_b representing the dimensionless temperature at the interface between the EDL and the bulk flow region. Therefore, the solution to Eq. (28) is

$$\Phi = e^{-a\overline{Y}}. \quad (29)$$

Eq. (29) indicates that the electric potential decays exponentially in the EDL. Following the work by Dutta and Beskok [32], we define the interface between the EDL and the bulk flow region at a location, at which the electric potential, Φ_b, decays one percent of the zeta potential, ζ. As a result, the thickness of the isothermal EDL is given by

$$\overline{Y}_b = 4.6052 \quad (y_b = 4.6052\lambda), \quad (30)$$

while for thermal EOFs, the thickness is

$$\overline{Y}_b = 4.6052/a \quad (y_b = 4.6052\lambda/a). \quad (31)$$

With Eq. (31), Eq. (27) can now be written as

$$U_b = 0.99 \frac{\bar{\varepsilon}_b}{\bar{\mu}_b} + \overline{Y}_b \frac{\lambda}{h} (\widetilde{\nabla} U^p \cdot \mathbf{n})_b. \quad (32)$$

As pointed out in the preceding section, the simplified model proposed in this work treats the electro-osmotic bulk flow as the flow of an electro-neutrality fluid. This means for a mixed electro-osmotic/pressure driven flow, its bulk flow behavior can be approximated as a Poiseuille flow with the identical pressure gradient. Therefore, U^p in Eq. (32) is indeed the velocity calculated in the simplified model. It follows that we can discard the superscript 'p' in Eq. (32) and rewrite it as

$$U_b = 0.99 \frac{\bar{\varepsilon}_b}{\bar{\mu}_b} + \overline{Y}_b \frac{\lambda}{h} (\widetilde{\nabla} U \cdot \mathbf{n})_b. \quad (33)$$

The corresponding dimensional form is

$$u_b = 0.99 u_s(T_b) + \overline{Y}_b \lambda (\nabla u \cdot \mathbf{n})_b, \quad (34)$$

where $u_s(T_b) = -\varepsilon(T_b)\zeta E/\mu(T_b)$, and $\nabla = \mathbf{i}\partial/\partial x + \mathbf{j}\partial/\partial y$.

Similarly, integrating Eq. (24) yields

$$\theta_b = \overline{Y}_b \frac{\lambda}{h} (\widetilde{\nabla}\theta \cdot \mathbf{n})_b + \overline{Y}_b^2 \frac{J\overline{K}_b}{2\bar{k}_b} \frac{\lambda^2}{h^2}, \quad (35)$$

and the corresponding dimensional form is given by

$$T_b - T_0 = \overline{Y}_b \lambda (\nabla T \cdot \mathbf{n})_b + \overline{Y}_b^2 \lambda^2 \frac{K(T_b)E^2}{2k(T_b)}. \quad (36)$$

It is clear from Eq. (36) that the temperature at the interface between the EDL and the bulk flow region, T_b, is related to the wall temperature, T_0.

Eqs. (33) and (35) are the dimensionless velocity and the dimensionless temperature at the interface between the electric double layer and the bulk flow region. As mentioned in Introduction, in the limit of $\gamma \gg 1$, since the EDL too small to be considered, the fluid flow and heat transfer in the entire microchannel can effectively be described by Eqs. (13)–(16) with the interfacial conditions, Eqs. (33) and (35). As a result, Eqs. (13)–(16), along with Eqs. (33) and (35), form a simple model for thermal EOFs in microchannels.

In addition, it is worth mentioning that although the model proposed in this work is derived in a two-dimensional straight microchannel, it can also be applied to other two-dimensional microstructures with a complex geometry, provided that the Debye length is much smaller than the local curvature of solid surfaces.

4. Lattice Boltzmann algorithm

We now present the double distribution function lattice Boltzmann method (DDF LBM) [44], a novel kinetic numerical algorithm, to numerically solve Eqs. (13)–(16).

In such a method, two basic distribution functions, the density distribution function f and the temperature distribution function g, are defined to describe the velocity field and the temperature distribution, respectively. For a two-dimensional problem, we can construct the DDF LBM from the Boltzmann equation with the BGK assumption on the following nine discrete particle velocities [49]:

$$\mathbf{c}_i = \begin{cases} (0,0) & i=0; \\ c(\cos[(i-1)\pi/2], \sin[(i-1)\pi/2]) & i=1,2,3,4; \\ \sqrt{2}c(\cos[(2i-9)\pi/4], \sin[(2i-9)\pi/4]) & i=5,6,7,8; \end{cases} \tag{37}$$

where $\mathbf{c}_i$ is the discrete particle velocity in the ith direction and c is the corresponding particle speed. The evolution equation for the density distribution function f is

$$f_i(\tau+\Delta\tau, \mathbf{X}+\mathbf{c}_i\Delta\tau) - f_i(\tau,\mathbf{X}) = -\omega[f_i(\tau,\mathbf{X}) - f_i^{\mathrm{eq}}(\tau,\mathbf{X})], \tag{38}$$

where f_i is the density distribution function in the ith particle velocity direction, τ, $\Delta\tau$ and $\mathbf{X}$ are the dimensionless time, the time step and the particle position, respectively. They are normalized by h/u_s (T_0) and h as in Eqs. (8)–(12). f_i^{eq} is the local density equilibrium distribution function and is given as

$$f_i^{\mathrm{eq}} = w_i\rho\left[1 + \frac{\mathbf{c}_i\cdot\mathbf{U}}{c_s^2} + \frac{\mathbf{c}_i\mathbf{c}_i:\mathbf{UU} - c_s^2\mathbf{I}:\mathbf{UU}}{2c_s^4}\right], \tag{39}$$

where the sound speed $c_s = \frac{\sqrt{3}c}{3}$, the weight coefficients $w_0 = \frac{4}{9}$; $w_i = \frac{1}{9}$, for $i = 1$–4; and $w_i = \frac{1}{36}$, for $i = 5$–8, and $\mathbf{I}$ is the second-rank unity tensor. In Eq. (38), ω is the dimensionless collision frequency for momentum. It can be evaluated by $\omega = 2c_s^2\Delta t/(2\bar{\mu}/Re + c_s^2\Delta t)$. The macroscopic density ρ, and the velocity $\mathbf{U}(U,V)$ are defined as

$$\rho = \sum_{i=0}^{8} f_i, \quad \rho\mathbf{U} = \sum_{i=0}^{8} f_i\mathbf{c}_i. \tag{40}$$

The temperature distribution is described by another distribution function g. When the heat source is present, its evolution equation is

$$g_i(\tau+\Delta\tau,\mathbf{X}+\mathbf{c}_i\Delta\tau) - g_i(\tau,\mathbf{X}) = -\omega_t[g_i(\tau,\mathbf{X}) - g_i^{\mathrm{eq}}(\tau,\mathbf{X})] + \Delta\tau S_i, \tag{41}$$

where g_i is the density distribution function in the ith particle velocity direction and the dimensionless collision frequency for energy $\omega_t = 2c_s^2\Delta t/[2\bar{k}/(Re\,Pr) + c_s^2\Delta t]$. g_i^{eq} is the local temperature equilibrium distribution function and is given as

$$g_i^{\mathrm{eq}} = \theta f_i^{\mathrm{eq}} = w_i\rho\theta\left[1 + \frac{\mathbf{c}_i\cdot\mathbf{U}}{c_s^2} + \frac{\mathbf{c}_i\mathbf{c}_i:\mathbf{UU} - c_s^2\mathbf{I}:\mathbf{UU}}{2c_s^4}\right]. \tag{42}$$

To describe the Joule heating in the thermal electro-osmotic flows in microchannels, S_i in Eq. (41) is specified as

$$S_i = w_i\frac{J\overline{K}}{Re\,Pr}\left[1 + \frac{\mathbf{c}_i\cdot\mathbf{U}}{c_s^2}\right]. \tag{43}$$

Then, we can obtain

$$\frac{J\overline{K}}{Re\,Pr} = \sum_{i=0}^{8} S_i, \qquad \frac{J\overline{K}\mathbf{U}}{Re\,Pr} = \sum_{i=0}^{8} S_i\mathbf{c}_i \tag{44}$$

Now the macroscopic temperature is defined by g_i:

$$\rho\theta = \sum_{i=0}^{8} g_i. \tag{45}$$

Through the Chapman–Enskog procedure [50], Eqs. (38), (39), (41) and (42), together with Eqs. (40) and (45), can recover the macroscopic mass, momentum and energy conservation equations.

In the DDF LBM, the variables through simulations are f and g, not the macroscopic velocity $\mathbf{U}$ and the temperature θ. Therefore, we should transform the boundary conditions of $\mathbf{U}$ and θ given by Eqs. (33)–(35) to the boundary conditions of f and g. We adopt the non-equilibrium extrapolation scheme [51]. For the boundary condition of the density distribution function, we obtain

$$f_i(\mathbf{X}_s) = f_i^{\mathrm{eq}}(\mathbf{U}_b,\rho^*) + f_i^{\mathrm{neq}}(\mathbf{X}_f), \tag{46}$$

where $\mathbf{X}_s$, and $\mathbf{X}_f$ denote the position of the nodes on the boundary and the position of the nodes in the fluid nearest the boundary, respectively, and f_i^{neq} is the non-equilibrium part of the density distribution function on $\mathbf{X}_f$ with the particle velocity in the ith direction. f_i^{eq} is given by Eq. (39) and the corresponding density $\rho^* = \rho(\boldsymbol{X}_f)$. For the temperature distribution function g, we construct its boundary condition as

$$g_i(\mathbf{X}_s) = g_i^{\mathrm{eq}}(\mathbf{U}_b,\theta_b,\rho^*) + g_i^{\mathrm{neq}}(\mathbf{X}_f), \tag{47}$$

where g_i^{eq} is given by Eq. (42) and g_i^{neq} is the non-equilibrium part of the temperature distribution function on $\mathbf{X}_f$ with the particle velocity in the ith direction.

5. Numerical results

In this section, we use the double distribution function lattice Boltzmann algorithm [44] to solve the simplified model given in the preceding section for the mixed electro-osmotic/pressure driven flows in microchannels. The numerical results from the complete model and the slip model with the HS velocity as the boundary condition at the solid walls are also presented.

5.1. Isothermal EOF

We first validate the present simplified model by simulating the isothermal mixed electro-osmotic/pressure driven flows in a two-dimensional straight microchannel with the width h and the length $L = 5h$, as shown in Fig. 1. It is

known under the isothermal condition, the fluid velocity component in x direction is analytically determined to be

$$U = U^{e} + U^{p}, \tag{48}$$

where U^{e} is the velocity component in x direction driven by the electro-osmosis while U^{p} is the one driven by the pressure gradient. For the flow with a large $\gamma = h/\lambda$, they are

$$U^{e} = 1.0 - (e^{-\gamma Y} + e^{-\gamma(1.0-Y)}), \tag{49}$$

and

$$U^{p} = \frac{dP/dX}{2}(Y^2 - Y). \tag{50}$$

We carried out our simulation on a $Nx \times Ny = 250 \times 50$ mesh. We arrange it in the bulk flow region between two interfaces denoting by two dashed lines shown in Fig. 1, i.e., $(h - 2y_b) \times L$, with y_b being the thickness of the EDL. We set the dimensionless pressure gradient $dP/dX = 3.0$ and the outlet dimensionless fluid density $\rho_{out} = 1.0$. The Reynolds number $Re = 0.01$ and the Prandtl number $Pr = 7.2$. We applied the pressure (density) boundary conditions [52] to the inlet/outlet and the non-equilibrium extrapolate scheme, i.e., Eqs. 46 and 47, to the upper and lower interfaces between the EDL and the bulk flow region.

Fig. 2 compares the resulting velocity profiles obtained from the present simplified model with the analytical solution given by Eq. (48) when $\gamma = 500$. It shows that the results given by the simplified model proposed in this work are in good agreement with the analytical solution over the entire bulk flow region, indicating that the model can be regarded as an accurate approximation for isothermal EOFs with a large γ. Fig. 2 also presents the results obtained from the complete model with inclusion of the EDL [45] and the slip model with the HS velocity as the boundary condition at the solid walls. It is seen that the velocity profile predicted by the complete model is identical to the analytical solution in both the EDL and the bulk flow region. However, it must be emphasized that, although accurate, the computation time using the complete model is about three times longer than that using the simplified model proposed in this work. Therefore, the complete model is inefficient for simulation of EOFs in microchannels. As to the slip model with the HS velocity, although it can qualitatively capture the basic feature of isothermal EOF, it is found that its numerical results deviate from the analytical solution with a relatively larger error in comparison with those from the present simplified model and the complete model. To present this point clearly, we define an average relative error of the streamwise velocity as

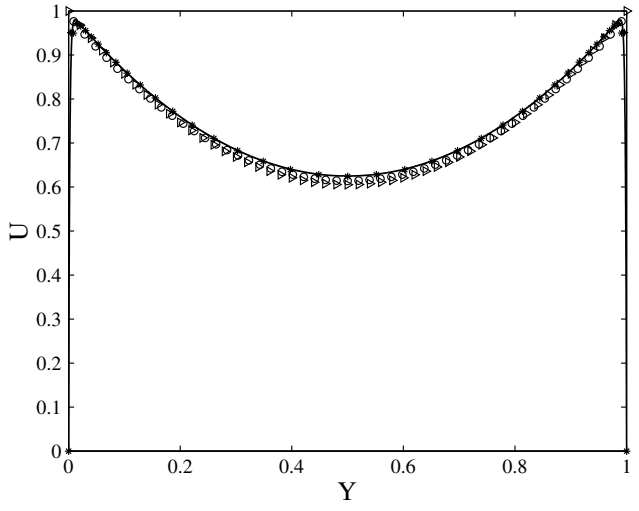

Fig. 2. The dimensionless streamwise velocity across the microchannel under the isothermal condition. (—) the analytical solution; (○) the simplified model proposed in this work; (∗) the complete model; (▷) the slip model with the HS velocity.

$$\Delta = \frac{1}{N_y}\sum_{i}\frac{|u(y_i) - \bar{u}(y_i)|}{\bar{u}(y_i)} \times 100\%, \tag{51}$$

where $u(y_i)$ and $\bar{u}(y_i)$ are the numerical results and the analytical solution given by Eq. (48), respectively; N_y is the number of grids distributed in y direction in the bulk flow region. It is found that in this case, the error given by the present model is 1.75% while that by the slip model with the HS velocity is 2%. Therefore, even in isothermal EOFs, the model proposed in this work can predict much more accurate velocity profile than that given by the slip model with the HS velocity.

5.2. Thermal EOF

We now present the results of simulation of the thermal mixed electro-osmotic/pressure driven flows. The computational region in this case is the same as that under the isothermal condition. We still conducted our simulation on a $Nx \times Ny = 250 \times 50$ mesh by setting $dP/dX = 3.0$, $\rho_{out} = 1.0$, $Re = 0.01$ and $Pr = 7.2$. We assumed that the fluid enters the channel with wall temperature and is thermally fully developed at the exit. The temperatures at the upper and lower interfaces are given by Eq. (35) and the Joule number $J = 1.0$. Moreover, in our simulation, the temperature dependent fluid properties are given by [45]

$$\varepsilon = 305.7\exp\left[-\frac{(\theta+1)T_0}{219}\right], \tag{52}$$

$$\mu = 2.761 \times 10^{-6}\exp\left[-\frac{1713}{(\theta+1)T_0}\right], \tag{53}$$

$$k = 0.61 + 0.0012\theta T_0, \tag{54}$$

and

$$K = K(T_0)[1 + 0.025T_0\theta], \tag{55}$$

where $T_0 = 298$ K.

Fig. 3 presents the resulting velocity profiles obtained by the present simplified model, the complete model and the slip model with the HS velocity for the thermal EOF systems with $\gamma = 200, 300, 400, 500$. It is seen that for the ther-

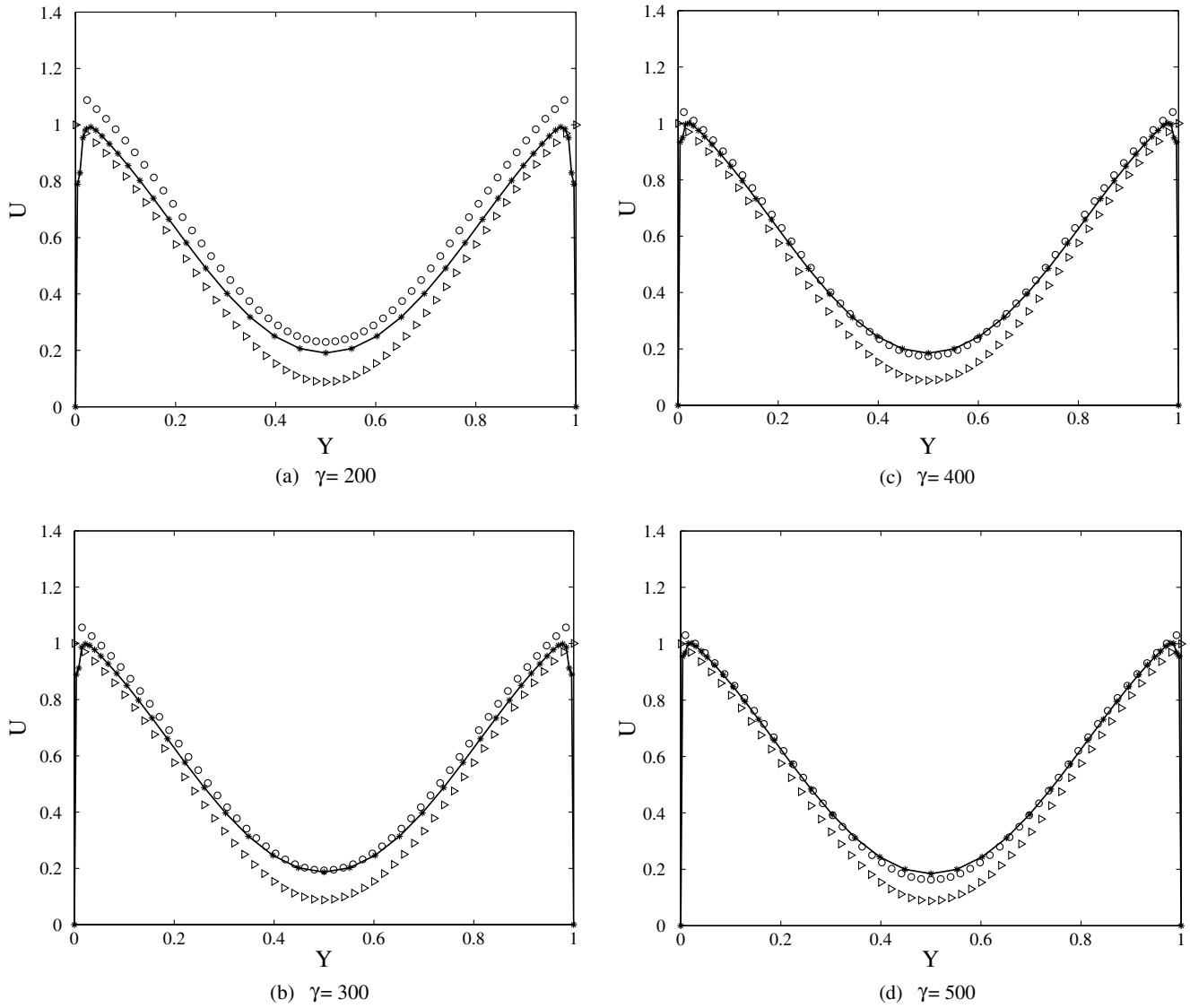

Fig. 3. The dimensionless streamwise velocity across the microchannel with $J = 1.0$. (-∗-) the complete model; (○) the simplified model proposed in this work; (▷) the slip model with the HS velocity.

mal EOF with a small length ratio γ (see Fig. 3a and b), the numerical results given by both the present model and the slip model with the HS velocity deviate substantially from that given by the complete model. Specifically, the slip model with the HS velocity as the boundary condition at the solid walls always predicts relatively smaller velocity while the model proposed in this work predicts a larger one. The underestimate in fluid velocity by the slip model with the HS velocity is due to the temperature-dependent fluid properties. As pointed out elsewhere [32], the HS velocity is obtained by extrapolating the bulk flow velocity onto the solid wall under the isothermal condition. It is evident that for flows with the thermal effect, the temperature-dependent fluid properties result in the different velocity profile from that under the isothermal condition. The HS velocity is no longer the extrapolation of the bulk flow velocity in a thermal EOF. Therefore, the simplification of the HS velocity as the boundary condition is inappropriate to thermal EOFs. On the other hand, in the model proposed in this work, we assume the temperature-dependent fluid properties in the EDL are constant and are equal to their values at the interface. It is evident that such an assumption is invalid for flows with a small γ, in which the EDL is relatively thicker and the fluid properties in this layer vary distinctly. As a result, we obtained a relative larger fluid velocity when γ is small. However, the accuracy of the present model improves with increasing the length ratio γ. Fig. 3c and d clearly shows that when $\gamma = 400$ and 500, the velocity profile given by this simplified model are in good agreement with that of the complete model. Such an improvement is because the EDL in these cases become sufficiently thin so that the fluid properties in this layer can be simply treated as constants. To more clearly compare the numerical results of the present model and the slip model with the HS velocity for thermal EOFs with different length ratios γ, we further calculated the numerical errors

Table 1
The numerical errors of the both slip models in thermal electro-osmotic flows with different length ratios γ

	The present model (%)	The slip model with HS velocity (%)
$\gamma = 200$	13.6	21.2
$\gamma = 300$	5.2	19.9
$\gamma = 400$	2.7	19.3
$\gamma = 500$	2.7	18.8

of the two models by Eq. (51), in which $\bar{u}$ is replaced by the numerical results obtained by the complete model. Table 1 presents the results. It is found that the errors of the both models are decreased as γ increases, demonstrating that the model with exclusion of the EDL is a reasonable approximation to the actual EOFs in the limit of a large length ratio, i.e., $\gamma \gg 1$. Moreover, we also found that although both the present model and the slip model with the HS velocity simplify the detail in the EDL as an effective boundary condition, the numerical error of the present model is much smaller than that of the slip model with the HS velocity for the EOF with a given γ. Taking the EOF with $\gamma = 400$ as an example, the numerical error of the present model is only 2.7% while that of the slip model with the HS velocity is up to 19.3%. Therefore, the simplified model proposed in this work can serve as a much more accurate tool for simulation of thermal EOFs with a large length ratio γ than the conventional slip model with the HS velocity.

Fig. 4 compares the corresponding temperature distributions obtained by the present model and the slip model with the HS velocity with those by the complete model for the thermal EOF systems with $\gamma = 200$, 300, 400 and 500. Being different from the velocity profiles, it is shown that the temperature distributions given by the three mod-

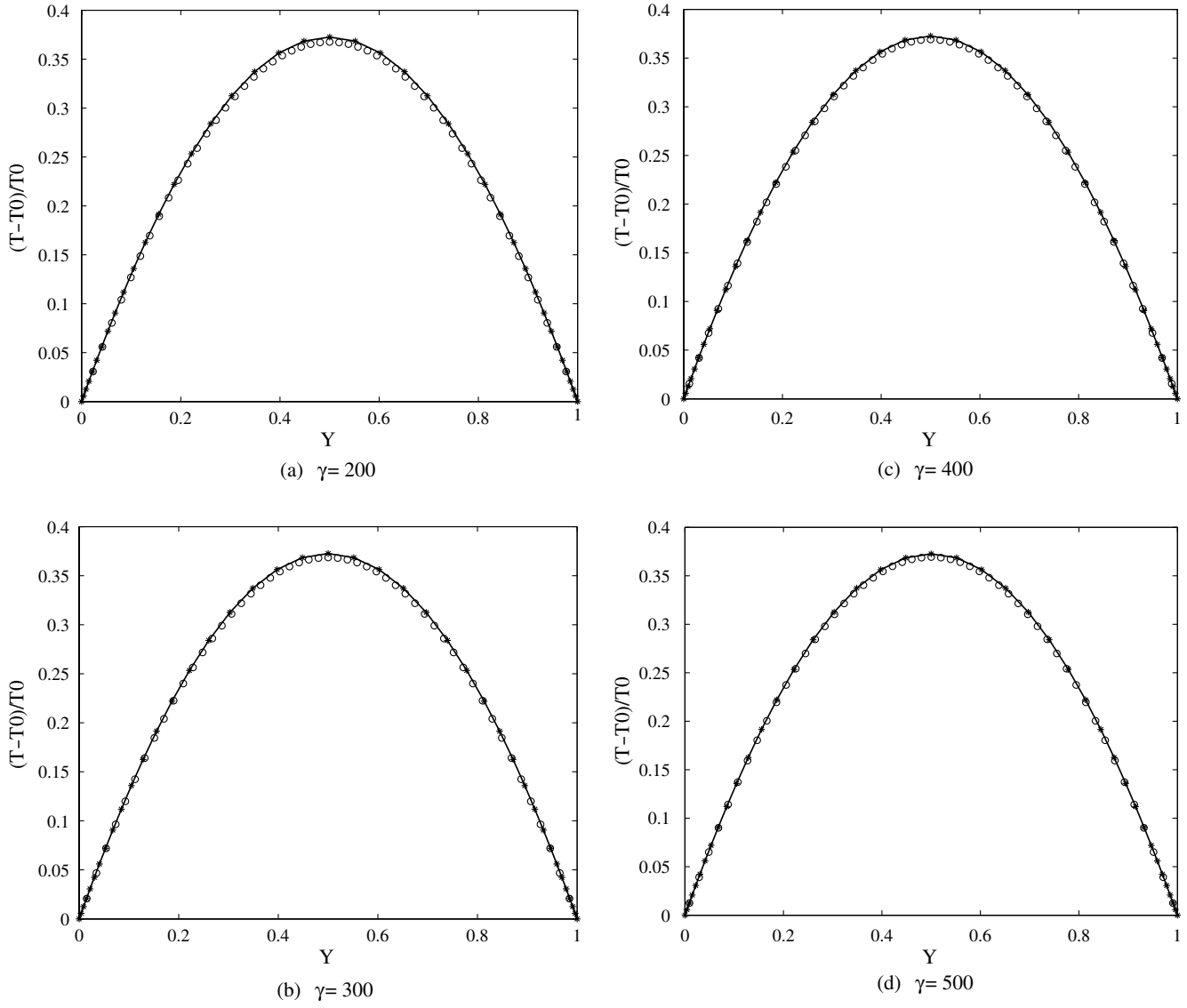

Fig. 4. The dimensionless temperature distribution across the microchannel with $J = 1.0$. (-∗-) the complete model; (○) the simplified model proposed in this work; (▷) the slip model with the HS velocity.

els are identical in all the cases with different length ratios, γ. It is also found that the distinct difference among velocity profiles given by the three models, as shown in Fig. 3, has a weak impact on the corresponding temperature distributions although the conservation equation of energy (7) is coupled with the Navier–Stokes equations (4) and (5). The reason for this interesting phenomenon is due to the very small Peclet number in the thermal electro-osmotic flows in microchannels. The results in Fig. 4 clearly indicate that both the present simplified model and the slip model with the HS velocity are capable of capturing the heat transfer characteristics in the EOFs in microchannels.

In addition, it is worth pointing out that as under the isothermal conditions, using the model proposed in this work would save substantially the computer memory and computational time as opposed with the complete model with inclusion of the EDL. For the thermal electro-osmotic flows with $\gamma = 400$, the computation time by the complete model with inclusion of the EDL was about five times longer than that using the proposed simplified model. Therefore, the model developed in this work is much more efficient than the complete model, which is demanded for the design and optimization of many more complex microfluidic systems.

6. Conclusion

In this paper, we have analytically derived the velocity and the temperature at the interface between the EDL and the bulk flow region. The Navier–Stokes equations and the conservation equation of energy, along with these interfacial velocity and temperature as the velocity-slip and temperature-jump boundary conditions, form a simple mathematical model for simulating the thermal EOF systems with a very thin EDL. We solved this model using the double distribution function lattice Boltzmann algorithm and compared the numerical results with those obtained by the complete model with inclusion of the EDL. We found that the present simplified model is in good agreement with the complete model particularly when the length ratio $\gamma \geqslant 400$. Moreover, the present model saves the computer memory and reduces significantly the computational time as opposed with the complete model. Therefore, the new model is more efficient for handling more complex EOF systems, which are demanded for the design and optimization of the microfluidic systems involving the electro-kinetic effect.

Acknowledgement

The work described in this paper was fully supported by a grant from the Research Grants Council of the Hong Kong Special Administrative Region, China (Project No. HKUST6101/04E).

References

[1] C.T. Culbertson, R.S. Ramsey, J.M. Ramsey, Electroosmotically induced hydraulic pumping on microchips: differential ion transport, Anal. Chem. 72 (2000) 2285–2291.
[2] A. Prochaska, Y. Nemirovsky, U. Dinnar, A membrane micropump electrostatically actuated across the working fluid, J. Micromech. Microeng. 15 (2005) 2309–2316.
[3] D.J. Laser, J.G. Santiago, A review of micropump, J. Micromech. Microeng. 14 (2004) R35–R64.
[4] C.H. Chen, J.G. Santiago, A planar electroosmotic micropump, J. Micromech. Microeng. 11 (2002) 672–683.
[5] I. Gitlin, A.D. Stroock, G.M. Whitesides, Pumping based on transverse electrokinetic effects, Appl. Phys. Lett. 83 (2003) 1486–1488.
[6] Z. Chen, P. Wang, H.C. Chang, An electro-osmotic micro-pump based on monolithic silica for micro-flow analyses and electrosprays, Anal. Bioanal. Chem. 382 (2005) 817–824.
[7] P. Wang, Z. Chen, H.C. Chang, A new electro-osmotic pump based on silica monoliths, Sens. Actuat. B 113 (2006) 500–509.
[8] S. Arulanandam, D. Li, Liquid transport in rectangular microchannels by electroosmotic pumping, Colloids Surf. A 161 (2000) 89–102.
[9] S.L. Zeng, C.H. Chen, J.C. Mikkelsen, J.G. Santiago, Fabrication and characterization of electroosmotic micropumps, Sens. Actuat. B 79 (2001) 107–114.
[10] M. Koch, A. Evans, A. Brunnschweiler, Microfluidic Technology and Applications, Research Studies Press, Philadelphia, PA, 2000.
[11] A. Ramos, A. Gonzalez, A. Castellanos, N.G. Green, H. Morgan, Pumping of liquids with ac voltages applied to asymmetric pairs of microelectrodes, Phys. Rev. E 67 (2003) 056302.
[12] A. Manz, C.S. Effenhauser, N. Burggraf, D.J. Harrison, K. Seiler, K. Fluri, Electroosmotic pumping and electrophoretic separation for miniaturized chemical analysis systems, J. Micromech. Microeng. 4 (1994) 257–265.
[13] V. Studer, A. Pepin, Y. Chen, A. Ajdari, Fabrication of microfluidic devices for AC electrokinetic fluid pumping, Microelectr. Eng. 61 (2002) 915–920.
[14] V. Studer, A. Pepin, Y. Chen, A. Ajdari, An integrated AC electrokinetic pump in a microfluidic loop for fast and tunable flow control, Analyst 129 (2004) 944–949.
[15] R.J. Yang, C.H. Wu, T.I. Tseng, S.B. Huang, G.B. Lee, Enhancement of electrokinetically-driven flow mixing in microchannel with added side channels, Jpn. J. Appl. Phys. 44 (2005) 7634–7642.
[16] C. Wang, Y. Gao, N.T. Nguyen, T.N. Wang, C. Yang, K.T. Ooi, Interface control of pressure-driven two-fluid flow in microchannels using electroosmosis, J. Micromech. Microeng. 15 (2005) 2289–2297.
[17] P. Dutta, A. Beskok, T.C. Warburton, Electroosmotic flow control in complex microgeometries, J. Microelectromech. Syst. 11 (2002) 36–44.
[18] N.A. Patankar, H.H. Hu, Numerical simulation of electroosmotic flow, Anal. Chem. 70 (1998) 1870–1881.
[19] D. Maynes, B.W. Webb, Fully developed electro-osmotic heat transfer in microchannels, Int. J. Heat Mass Transfer 46 (2003) 1359–1369.
[20] B.C. Liechty, B.W. Webb, R.D. Maynes, Convective heat transfer characteristics of electro-osmotically generated flow in microtubes at high wall potential, Int. J. Heat Mass Transfer 48 (2005) 2360–2371.
[21] D. Maynes, B.W. Webb, Fully-developed thermal transport in combined pressure and electro-osmotically driven flow in microchannels, J. Heat Transfer 125 (2003) 889–895.
[22] C. Yang, D. Li, J.H. Masliyah, Modeling forced liquid convection in rectangular microchannels with electrokinetic effects, Int. J. Heat Mass Transfer 41 (1998) 4229–4249.
[23] T.S. Zhao, Q. Liao, Thermal effects on electro-osmotic pumping of liquids in microchannels, J. Micromech. Microeng. 12 (2002) 962–970.

[24] A.D. Stroock, M. Weck, D.T. Chiu, W.T.S. Huck, P.J.A. Kenis, R.F. Ismagilov, G.M. Whitesides, Patterning electro-osmotic flow with patterned surface charge, Phys. Rev. Lett. 84 (2000) 3314–3317.
[25] A. Ajdari, Pumping liquids using asymmetric electrode arrays, Phys. Rev. E 61 (2000) R45–R48.
[26] J.S. Newman, Electrochemical Systems, Prentice Hall, New Jersey, 1991.
[27] R. Qian, N.R. Aluru, A compact model for electroosmotic flows in microfluidic devices, J. Micromech. Microeng. 12 (2002) 625–635.
[28] X. Xuan, D. Sinton, D. Li, Thermal end effects on electroosmotic flow in a capillary, Int. J. Heat Mass Transfer 47 (2004) 3145–3157.
[29] X. Xuan, B. Xu, D. Sinton, D. Li, Electroosmotic flow with Joule heating effects, Lab Chip 4 (2004) 230–236.
[30] J.S.H. Lee, Y. Hu, D. Li, Electrokinetic concentration gradient generation using a converging-diverging microchannel, Anal. Chim. Acta 543 (2005) 99–108.
[31] M.H. Chang, G.M. Homsy, Effects of Joule heating on the stability of time-modulated electro-osmotic flow, Phys. Fluids 17 (2005) 074107.
[32] P. Dutta, A. Beskok, Analytical solution of combined electroosmotic/pressure driven flows in two-dimensional straight channels: finite Debye layer effects, Anal. Chem. 73 (2001) 1979–1986.
[33] G.E. Karniadakis, A. Beskok, Micro Flows: Fundamental and Simulation, Springer Verlag, New York, 2002.
[34] G. Gouy, Sur la constitution de la charge électrique à la surface d'un electrolyte, J. Phys. 9 (1910) 457–468.
[35] R.F. Probstein, Physicochemical Hydrodynamics: An Introduction, John Wiley, New York, 1994.
[36] D. Erickson, D. Sinton, D. Li, Joule heating and heat transfer in poly(dimethylsiloxane) microfluidic systems, Lab. Chip 3 (2003) 141–149.
[37] K.L.K. Liu, K.L. Davis, M.D. Morris, Raman spectroscopic measurement of spatial and temporal temperature gradients in operating electrophoresis capillaries, Anal. Chem. 66 (1994) 3744–3750.
[38] D.S. Burgi, K. Salomon, R.L. Chien, Methods for calculating the internal temperature of capillary columns during capillary electrophoresis, J. Liq. Chromatogr. 14 (1991) 847–867.
[39] Y. Wang, Q. Lin, T. Mukherjee, A model for Joule heating-induced dispersion in microchip electrophoresis, Lab. Chip 4 (2004) 625–631.
[40] J.H. Knox, K.A. McCormack, Temperature effects in capillary electrophoresis. 2. Some theoretical calculations and predictions, Chromatographia 38 (1994) 215–221.
[41] A.J. de Mello, Control and detection of chemical reactions in microfluidic systems, Nature 442 (2006) 394–402.
[42] G. Hu, Q. Xiang, R. Fu, B. Xu, R. Venditti, D. Li, Electrokinetically controlled real-time polymerase chain reaction in microchannel using Joule heating effect, Anal. Chim. Acta 557 (2006) 146–151.
[43] I.T. Gorbachuk, V.P. Dushchenko, V.P. Sergienko, R.M. Kotsyuba, Effect of temperature on the state of boundary and electric double layers, Colloid J. USSR 50 (1989) 557–562 (English translation of Kolloidnyi Z).
[44] Y. Shi, T.S. Zhao, Z.L. Guo, Thermal lattice Bhatnagar–Gross–Krook model for flows with viscous heat dissipation in the incompressible limit, Phys. Rev. E 70 (2004) 066310.
[45] Z.L. Guo, T.S. Zhao, Y. Shi, A lattice Boltzmann algorithm for electro-osmotic flows in microfluidic devices, J. Chem. Phys. 122 (2005) 144907.
[46] J.N. Israelachvili, Intermolecular and Surface Forces, Academic Press, San Diego, 1991.
[47] J.K. Wang, M. Wang, Z.X. Li, Lattice Poisson–Boltzmann simulations of electro-osmotic flows in microchannels, J. Colloid Interf. Sci. 296 (2006) 729–736.
[48] G.H. Tang, Z. Li, J.K. Wang, Y.L. He, W.Q. Tao, Electroosmotic flow and mixing in microchannels with the lattice Boltzmann method, J. Appl. Phys. 100 (2006) 094908.
[49] Y.H. Qian, D. D'Humières, P. Lallemand, Lattice BGK models for Navier–Stokes equation, Europhys. Lett. 17 (1992) 479–484.
[50] S. Chapman, T.G. Cowling, The Mathematical Theory of Non-Uniform Gases: An Account of the Kinetic Theory of Viscosity, Thermal Conduction and Diffusion in Gases, Cambridge University Press, Cambridge, 1990.
[51] Z.L. Guo, C.G. Zheng, B.C. Shi, An extrapolation method for boundary conditions in lattice Boltzmann method, Phys. Fluids 14 (2002) 2007–2010.
[52] Z.L. Guo, C.G. Zheng, B.C. Shi, Non-equilibrium extrapolation method for velocity and pressure boundary conditions in the lattice Boltzmann method, Chin. Phys. 11 (2002) 366–374.